Optical conductivity of perovskite manganites

Nandan Pakhira,[1,2,*] H. R. Krishnamurthy,[1,2] and T. V. Ramakrishnan[1,2,3]

[1]*Centre for Condensed Matter Theory, Department of Physics, Indian Institute of Science, Bangalore 560 012, India*

[2]*Condensed Matter Theory Unit, Jawaharlal Nehru Centre for Advanced Scientific Research, Bangalore 560 064, India*

[3]*Department of Physics, Banaras Hindu University, Varanasi 221 005, India*

(Received 18 September 2009; revised manuscript received 20 June 2011; published 22 August 2011)

We calculate the optical conductivity $\sigma(\omega)$ for doped rare-earth manganites based on the recently proposed microscopic "two fluid" $\ell-b$ model. We study the temperature dependence of $\sigma(\omega)$ for $La_{0.825}Sr_{0.175}MnO_3$, which has a metallic ground state. At low temperatures, the calculated $\sigma(\omega)$ shows a "two-peak" structure consisting of a far-infrared coherent Drude peak and a broad mid-infrared "polaron" peak, as observed in experiments. Upon heating, the Drude peak rapidly loses spectral weight, and $\sigma(\omega)$ crosses over to having just a single broad mid-infrared peak. The temperature dependence of the mid-infrared peak and the spectral weight transfer between the two peaks are also in agreement with experimental findings. We also study the doping dependence of $\sigma(\omega)$ for the same compound. The integrated spectral weight under the Drude peak increases rapidly as the doping level is increased from an underdoped, insulating state ($x = 0.1$) to a highly doped, metallic state ($x = 0.3$), again in agreement with trends seen experimentally.

DOI: 10.1103/PhysRevB.84.085115 PACS number(s): 75.47.Lx, 71.38.−k, 78.20.−e, 71.27.+a

I. INTRODUCTION

The discovery[1] of colossal magnetoresistance (CMR) phenomena in alkaline-earth doped rare-earth manganites $Re_{1-x}A_xMnO_3$ (Re is a rare-earth atom, e.g., La, Nd, Pr, and A is an alkaline-earth atom, e.g., Ca, Sr, Ba) triggered an explosion of activity in the exploration of their properties,[2–5] reviving interest in these rather old systems.[6] The parent compound, e.g., $LaMnO_3$, is a Mott insulator with an A-type antiferromagnetic ground state. When divalent cations, e.g., Ca, Sr, etc., are substituted for La, the resulting materials show a rich variety of electronic and magnetic phases and properties depending on the doping level x and the cation (characterized, e.g., by its radius), including such intriguing phenomena like CMR, different types of charge, orbital and magnetic ordering, metal insulator transitions, and nanoscale and mesoscale phase separation.

The optical properties of the doped manganites are also very interesting and puzzling (see Refs. 7–12 and numerous other references from the review articles cited above[2–5]). Typically, at sufficiently low temperatures $T \ll T_c$ (the magnetic ordering temperature), the optical conductivity $\sigma(\omega)$ in the metallic phase consists of two major features. First, a Drude-like (approximately half Lorentzian) peak in the far-infrared region with an anomalously small integrated weight, amounting to less than 10% of the carrier number;[7,8] second, a broad peak or shoulder in the mid-infrared region ($\hbar\omega \approx 1$ eV) often attributed to polarons (e.g., see Refs. 9 and 11). As the temperature increases, there is transfer of spectral weight over a frequency or energy region much larger than the temperature, e.g., from the Drude peak to the mid-infrared peak. If the high-temperature phase is a metal, a weak Drude peak is still present at high temperatures; whereas if it is an insulator, there is no Drude peak. In recent measurements[12] on manganite samples with *cleaved* surfaces (rather than on those with *polished* surfaces as in the experiments mentioned above) it has been suggested that $\sigma(\omega)$ is better described with a single curve with a nonintegral power law $\omega^{-\nu}$ rather than in terms of a small Drude peak and a broad mid-infrared peak.[13] On the other hand, measurements on thin-film systems[14,15] show that the optical conductivity is dominated by a broad mid-infrared peak. The thin-film systems are inherently more disordered in nature (due to surface strain effects, etc.) and hence coherent features like a Drude peak in the far-infrared region can have very low spectral weight.

In this paper, using the *two-fluid* $\ell-b$ picture proposed and developed in a series of recent papers,[16–23] we present detailed calculations for the optical conductivity of doped manganites, which capture many of the key features of the experimental data discussed above. Needless to say, there have been many earlier theoretical papers[24–33] aimed at describing the optical properties of manganites. We present a detailed discussion of these *vis-a-vis* our work later (see Sec. IV) in this paper.

The two-fluid $\ell-b$ model[17–19,21] pictures the $(1-x)$ e_g electrons (per site) in the doped manganite as spontaneously reorganizing themselves into two interpenetrating fermionic fluids, the large majority being a collection of localized small polarons (ℓ_j) self-trapped on sites accompanied by large Jahn-Teller distortions, and a small minority being mobile band electrons (b_i) hopping around on nearly undistorted Mn sites avoiding the ℓ polarons. It has been shown that this model explains a number of the characteristic properties of manganites, e.g., colossal magnetoresistance,[17] ubiquitous metal-insulator transitions induced by doping[16] or by temperature,[17] nanoscale phase separation,[22] and anomalous temperature-dependent photoemission satellites.[23] We use this same model (described in greater detail in Sec. II) here for a calculation of the optical properties of doped manganites for different hole doping x and temperature T (Sec. III). We find that the real part of the frequency-dependent optical conductivity $\sigma(\omega)$ indeed has a Drude-like feature, originating mainly from the b electrons, and a far-infrared peak or shoulder, connected with the ℓ polarons. Furthermore, there is a dramatic transfer of spectral weight from the former to the latter as the temperature increases and crosses T_c, the magnetic (as well as metal-insulator[34]) transition temperature. The results are expected to be directly applicable to the orbital

fluid regime of doped manganites (e.g., $La_{1-x}Ca_xMnO_3$ for $0.1 < x < 0.4$) under conditions when the quantum coherence between the polarons and the mobile electrons is suppressed. We present our results and compare them with experiments in Sec. IV, where we also discuss at some length the earlier theoretical work *vis-à-vis* our work. The concluding section (Sec. V) mentions some open questions and ways in which the present calculations need to be and can be further improved.

II. TWO-FLUID $\ell-b$ MODEL

The $\ell-b$ model is represented by the following Hamiltonian:

$$H_{\ell b} = \sum_{i,\sigma}(\epsilon_\ell - \mu)\, n_{\ell i\sigma} - \mu \sum_{j,\sigma} b^\dagger_{j\sigma} b_{j\sigma} - \sum_{\langle jj'\rangle\sigma} \bar{t}_{jj'} b^\dagger_{j\sigma} b_{j'\sigma} + U_{\ell b} \sum_{i,\sigma,\sigma'} n_{\ell i\sigma} n_{bi\sigma'} - J_H \sum_i (\vec{s}_{\ell i} + \vec{s}_{bi}) \cdot \vec{S}_i - \bar{J}_F \sum_{\langle ij\rangle} \vec{S}_i \cdot \vec{S}_j. \quad (1)$$

Here, $n_{\ell i\sigma}$ is the number operator for an e_g electron self-trapped in a localized *polaronic* state centered at a site i with a local Jahn-Teller (JT) distortion, and E_{JT} ($\equiv -\epsilon_\ell$) denotes the binding energy of the polaron. $b^\dagger_{j\sigma}$ creates mobile e_g electrons that hop primarily among undistorted sites j, j' with some average amplitude $\bar{t}_{jj'}$ (see the Appendix for details); they are kept away from the distorted sites where the ℓ polarons reside by the large Coulomb repulsion term $U_{\ell b}$. The chemical potential μ is adjusted to ensure the constraint (due to the doping) that the average number of e_g electrons per site must equal $(1-x)$:

$$N^{-1}\sum_i \langle n_i\rangle \equiv N^{-1}\sum_i\sum_\sigma (\langle n_{\ell i\sigma}\rangle + \langle n_{bi\sigma}\rangle) = (1-x). \quad (2)$$

For simplicity we have not explicitly exhibited in Eq. (1) the other Coulomb interactions that are present, such as U_{bb} and $U_{\ell\ell}$. Because the b electrons are itinerant, and, as we show later, their concentration is sufficiently small in the doping regions, in our work we focus on the fact that the effect of the U_{bb} term can be treated within a Hartree-Fock (HF) approximation, which just renormalizes the chemical potential. The local ℓ electron occupation number $n_{\ell i} \equiv \sum_\sigma n_{\ell i\sigma}$ is a conserved quantity and has values 0, 1, and 2. We include the effect of a large $U_{\ell\ell}$ by simply excluding the configurations with $n_\ell = 2$. Only $U_{\ell b} \equiv U$, which is shown explicitly in Eq. (1), plays a nontrivial role and is also the highest energy scale (5–10 eV as estimated from photoemission[35] and band-structure calculations[36]) in the problem. $\bar{J}_F$, the effective ferromagnetic coupling between the t_{2g} "core spins" $\vec{S}_i$ on the Mn sites, arises from the "virtual double exchange"[17–19,21,37] mechanism, due to the fast (nonadiabatic) virtual hopping of an ℓ electron to a nearest-neighboring site and back, leaving the local lattice distortion unrelaxed, by paying a lattice energy cost of $2E_{JT}$ in the intermediate state, provided that the neighboring site is empty and the t_{2g} core spins at the two sites are parallel to each other. For $E_{JT} \gg \bar{t}$, this process gives rise to a new, ℓ occupancy dependent (x dependent), ferromagnetic exchange coupling between the t_{2g} core spins of the form

$$J_F = \left[\frac{\bar{t}^2}{2E_{JT}S^2}\right][n_{\ell i}(1-n_j) + n_{\ell j}(1-n_i)]. \quad (3)$$

For the purposes of this work, where the doping regimes explored involve no charge ordering, we have replaced this by an averaged ferromagnetic coupling $\bar{J}_F \sim \bar{t}^2 x(1-x)/(E_{JT}S^2)$, and use it as an adjustable parameter.[38] J_H is the ferromagnetic Hund's coupling between the core spin at a site i and the spin of the e_g electron at the same site, whether it is that of the ℓ polaron ($\vec{s}_{\ell i}$) or of the b electron ($\vec{s}_{bi}$). It is large (~2 eV) and essentially forces the spin of the e_g electron to be aligned with the core spin.

Although the $\ell-b$ model so far not been *rigorously derived* from a microscopic Hamiltonian, there are fairly compelling arguments one can make[17–19,21] as to why it is the appropriate low-energy Hamiltonian in the orbital liquid regime (albeit with parameters renormalized from their bare values) even when E_{JT} is of order t so that the bare bandwidth $D_0 \gg E_{JT}$. For, due to the competing effects of the various strong interactions present and the filling constraints, the kinetic-energy gain, by having the e_g electrons mobile, gets suppressed, so the majority of the electrons would rather become localized polarons and gain JT energy. The t_{2g} core spins are large enough ($S = 3/2$) that they can be well approximated as classical spins $S\hat{\Omega}_i$ of length S, where $\hat{\Omega}_i$ are unit vectors that point anywhere on a unit sphere. In that case, $H_{\ell b}$ is similar to the well-known Falicov-Kimball[39] model (FKM) for nonhybridizing localized (f) electrons interacting with itinerant (d or p) electrons. At $T = 0$, in the ferromagnetic phase, it in fact reduces to the FKM. The b electrons move around in the presence of an annealed random medium, strongly repelled (repulsion U) from sites with static ℓ electrons; hence for large U their amplitude is largest on the undistorted sites unoccupied by the polarons. At $T \neq 0$, there is also annealed randomness in $\hat{\Omega}_i$, which scatters b electrons via J_H. If we assume that the annealed randomness is homogeneous, i.e., $\bar{n}_{\ell i} = \bar{n}_\ell$ and $\bar{n}_{bi} = \bar{n}_b$ such that $\bar{n}_\ell + \bar{n}_b = (1-x)$ and that $\langle\hat{\Omega}_i\rangle = m$, then even for strong U and J_H, one can solve this problem[16,17,37] within the approximation of dynamical mean-field theory (DMFT),[40] which is exact at dimensionality $d = \infty$, and is quite accurate for $d = 3$. As mentioned earlier, the results for thermodynamic, spectral, and transport properties, even in the simpler $J_H \to \infty$ limit, give an excellent account of the properties of manganites. The results for a realistic tight-binding band structure and a semicircular density of states with bare half bandwidth D_0 are close to each other (for details, see Ref. 37). Hence in this work[41] we study the frequency-dependent conductivity, i.e., the optical conductivity $\sigma(\omega)$ of the $\ell-b$ model in the same framework, i.e., using the propagators for the ℓ polarons and b electrons obtained within the DMFT, in the $J_H \to \infty$ limit and using a semicircular density of states.

III. OPTICAL CONDUCTIVITY IN THE $\ell-b$ MODEL

The optical conductivity $\sigma^{\mu\nu}(\omega)$ is the *linear response* of the current operator $j^{\mu}(\omega)$ to an externally applied electric field **E**,

$$\langle j^{\mu}(\omega)\rangle = \sigma^{\mu\nu}(\omega)E_{\nu}(\omega). \tag{4}$$

For a system without any *of-diagonal long-range order* (ODLRO) (such as superconductivity), the real part of conductivity tensor $\sigma^{\mu\nu}(\omega)$ is given by[42]

$$\sigma_R^{\mu\nu}(\omega) = \frac{e^2}{\omega}\mathrm{Im}[\chi^{\mu\nu}(\omega^+)], \tag{5}$$

where $\chi^{\mu\nu}(\omega)$ is the *retarded current-current correlation function* defined as

$$\chi^{\mu\nu}(\omega) = -\frac{i}{\hbar}\int_{-\infty}^{+\infty} dt\ \Theta(t)e^{i\omega t}\langle[j^{\mu}(t), j^{\nu}(0)]\rangle. \tag{6}$$

Equivalently, it can be calculated for the even Matsubara frequencies, $i\nu_m \equiv 2\pi m k_B T$, in a thermal Green's function or Matsubara formalism as

$$\begin{aligned}\chi^{\mu\nu}(i\nu_m) &= \int_0^{\beta} d\tau\ e^{i\nu_m\tau}\Pi^{\mu\nu}(\tau);\\ \Pi^{\mu\nu}(\tau) &= -\frac{1}{v}\langle T_{\tau}[j^{\mu}(\tau)j^{\nu}(0)]\rangle\end{aligned} \tag{7}$$

and then analytically continued to real frequencies.[42] In order to proceed with its calculation within the $\ell-b$ model, we need to model the current operator j^{μ} within the same framework.

The current operator will clearly have contributions from both types of electrons. The contribution from the b electrons, which we denote j_{bb}, is the easiest to model. Consistent with Eq. (1) according to which the b electrons hop around with amplitudes $\bar{t}_{jj'}$ on the undistorted sites of the lattice, one has the standard expression[42]

$$j_{bb}^{\mu} = \frac{i}{2\hbar}\sum_{\langle i,j\rangle}\bar{t}_{ij}R_{ij}^{\mu}(b_{i\sigma}^{\dagger}b_{j\sigma} - b_{j\sigma}^{\dagger}b_{i\sigma}). \tag{8}$$

The second important contribution to the current operator, which we label $j_{\ell b}$, arises from the fast motion of an ℓ *electron* (i.e., leaving the lattice distortion at its site frozen) to a neighboring undistorted site, i.e., as a b electron. Similarly to the above, we write (see the Appendix for details)

$$\begin{aligned}j_{\ell b}^{\mu} = \frac{i}{2\hbar}\alpha_{\ell b}\sum_{\langle i,j\rangle}\bar{t}_{ij}R_{ij}^{\mu}[(\ell_{ei\sigma}^{\dagger}b_{j\sigma} - b_{j\sigma}^{\dagger}\ell_{ei\sigma})\\ + (b_{i\sigma}^{\dagger}\ell_{ej\sigma} - \ell_{ej\sigma}^{\dagger}b_{i\sigma})].\end{aligned} \tag{9}$$

Here, for clarity, we have added a subscript e to the ℓ *electron* creation and destruction operators to distinguish them from the operators for creating and destroying the ℓ polarons. Furthermore, we have multiplied the expression for $j_{\ell b}$ by a semiphenomenological parameter $\alpha_{\ell b} \lesssim 1$ in order to compensate for the limitations of our modeling and calculations, for the b electrons are effective degrees of freedom that represent in an averaged way the e_g electrons of both orbital types on the undistorted sites, whereas the ℓ electrons are trapped in specific orbital combinations that are consistent with the "orientations" of the JT distortions at their sites (see the Appendix for details). The modeling and the approximate DMFT treatment we use below to calculate their current current correlations do not capture accurately the relevant short-range and short-time constraints on their orbital correlations and the effects arising from the avoidance of the ℓ polarons by the b electrons. Furthermore, in our modeling we have completely neglected $\ell-b$ hybridization effects. $\alpha_{\ell b}$ can in principle vary with temperature and doping, but a microscopic theory that allows one to calculate it taking into account all the factors that are responsible presents tremendous theoretical challenges. For the purposes of the present study we treat it as an adjustable constant.

We do not consider currents of the form $j_{\ell\ell}$, which involve the hopping of an ℓ *electron* to a neighboring site which is also distorted, whence it is likely to be occupied in the initial state and hence all contributions to $\sigma(\omega)$, the optical conductivity, will involve energy costs of local double occupancy and will have spectral weights only at very large energy scales (of order U, corresponding to excitations to the upper Hubbard bands).

Thus within the above level of modeling, where we ignore quantum coherent hybridization between the ℓ polarons and the b electrons, and at the energy scales of our interest, $\chi^{\mu\nu}(i\nu_m)$ can be expressed as the sum

$$\chi^{\mu\nu}(i\nu_m) = \chi_{bb}^{\mu\nu}(i\nu_m) + \chi_{\ell b}^{\mu\nu}(i\nu_m) + \chi_{b\ell}^{\mu\nu}(i\nu_m). \tag{10}$$

In Fig. 1 we have shown, diagrammatically, the contributions arising from the diagonal $b-b$ channel and the off-diagonal $\ell-b$ channels. In the first process, the oscillatory time-dependent transport of b electrons generating particle-hole excitations on undistorted sites directly contributes to the optical conductivity, termed $\sigma_{bb}(\omega)$. In the other processes, contributing to $\sigma_{\ell b}(\omega)$, ℓ polarons get excited to a b-like state on neighboring undistorted sites by temporarily unbinding from their polaronic clouds, analogous to the Frank-Condon excitation processes known in molecular spectra.

The total optical conductivity $\sigma(\omega)$ is then given by

$$\sigma(\omega) = \sigma_{bb}(\omega) + \sigma_{\ell b}(\omega), \tag{11}$$

where

$$\sigma_{bb/\ell b}(\omega) = \frac{\mathrm{Im}[\chi_{bb/\ell b}(\omega + i\delta)]}{\omega} \tag{12}$$

$$\begin{aligned}\text{with}\quad \chi_{bb}(i\nu_m) = -\frac{1}{N\beta}\sum_{\mathbf{k}}v_{\mathbf{k}x}^2\sum_{\sigma}\sum_{n}G_{bb}^{\sigma}(\epsilon_{\mathbf{k}}, i\omega_n)\\ \times G_{bb}^{\sigma}(\epsilon_{\mathbf{k}}, i\nu_m + i\omega_n)\end{aligned} \tag{13}$$

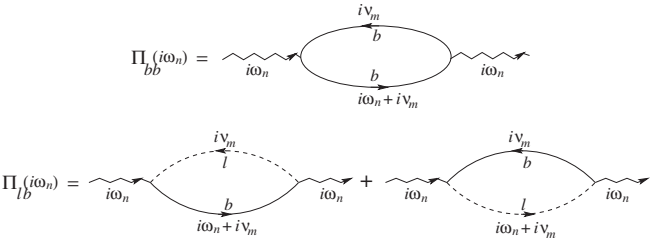

FIG. 1. Two independent bubble diagram contributions to the optical conductivity.

$$\chi_{\ell b}(i\nu_m) = -\frac{(\alpha_{\ell b})^2}{2N\beta}\sum_{\mathbf{k}} v_{\mathbf{k}x}^2 \sum_{\sigma}\sum_{n}\left[G^{\sigma}_{\ell_e\ell_e}(i\omega_n)G^{\sigma}_{bb}(\epsilon_{\mathbf{k}},i\nu_m + i\omega_n) + G^{\sigma}_{bb}(\epsilon_{\mathbf{k}},i\omega_n)G^{\sigma}_{\ell_e\ell_e}(i\nu_m + i\omega_n)\right]. \quad (14)$$

Here,

$$G^{\sigma}_{bb}(\epsilon_{\mathbf{k}},i\omega_n) = \frac{1}{i\omega_n + \mu - \epsilon_{\mathbf{k}} - \Sigma^{\sigma}_{bb}(i\omega_n)} \quad (15)$$

is the single-particle propagator of the b electron with momentum $\mathbf{k}$ and spin index σ (which can be up or down), which is dependent only on $\epsilon_{\mathbf{k}}$, as its self-energy $\Sigma^{\sigma}_{bb}(i\omega_n)$ is evaluated within the DMFT and is hence local and only frequency dependent. Their features have been discussed in detail elsewhere.[16,17,37] $G^{\sigma}_{\ell_e\ell_e}(i\omega_n)$ is the ℓ *electron* propagator. In contrast to the b propagator, within the framework of our modeling the ℓ electron propagator is purely local, and does not have a momentum dependence. We discuss it further below.

By using standard techniques[42] to evaluate the summations over the *odd* Matsubara frequencies above, we get

$$\sigma_{bb}(\omega) = \frac{\pi e^2}{\hbar a}\int_{-\infty}^{+\infty} D^{bb}_{tr}(\epsilon)d\epsilon \int_{-\infty}^{+\infty} d\omega' \sum_{\sigma} A^{\sigma}_{bb}(\epsilon,\omega')A^{\sigma}_{bb}(\epsilon,\omega+\omega')\left[\frac{n_F(\omega') - n_F(\omega'+\omega)}{\omega}\right], \quad (16)$$

$$\sigma_{\ell b}(\omega) = \frac{\pi e^2(\alpha_{\ell b})^2}{2\hbar a}\int_{-\infty}^{+\infty} D^{bb}_{tr}(\epsilon)d\epsilon \int_{-\infty}^{+\infty} d\omega' \sum_{\sigma}\left[A^{\sigma}_{\ell_e\ell_e}(\omega')A^{\sigma}_{bb}(\epsilon,\omega'+\omega) + A^{\sigma}_{\ell_e\ell_e}(\omega'+\omega)A^{\sigma}_{bb}(\epsilon,\omega')\right]\left[\frac{n_F(\omega') - n_F(\omega'+\omega)}{\omega}\right]. \quad (17)$$

Here $A^{\sigma}_{bb}(\epsilon,\omega) = -\frac{1}{\pi}\mathrm{Im}[G^{\sigma}_{bb}(\epsilon,\omega^+)]$ is the energy-dependent single-particle spectral function of the b electrons, $A^{\sigma}_{\ell_e\ell_e} = -\frac{1}{\pi}\mathrm{Im}[G^{\sigma}_{\ell_e\ell_e}(\omega^+)]$ is the spectral function for the ℓ *electrons*, $n_F(\omega) \equiv 1/[1+\exp(\beta\omega)]$ is the Fermi function, and a is the lattice spacing. $D^{bb}_{tr}(\epsilon)$ is the *transport density of states* for the b electrons[43] defined as

$$D^{bb}_{tr}(\epsilon) \equiv \frac{1}{N}\sum_{\mathbf{k}} v^2_{\mathbf{k}x}\delta(\epsilon - \epsilon_{\mathbf{k}}). \quad (18)$$

For the hypercubic lattice in infinite dimensionality it is proportional to the *bare density of states* $D_0(\epsilon)$ and is given by $D^{bb}_{tr}(\epsilon) = t^2 D_0(\epsilon)$. Hence we use this relation for the purposes of our work, although for simplicity we use the semicircular density of states (DOS) for $D_0(\epsilon)$.

$G^{\sigma}_{\ell_e\ell_e}(\omega)$ in the above equations is the Green's function for the ℓ *electrons* with spin σ, which can be obtained from the "polaronic" ℓ state by deconvoluting its polaronic cloud. The two terms in Eq. (17) correspond to the two processes in which ℓ *electron* is either being removed from or put into a distorted site. As already mentioned, the ℓ states that arise due to strong coupling of orbitally degenerate e_g electrons to JT distortion are polaronic in nature, and cannot take part directly in real transport phenomena. Currents are carried by the original electrons in one of the twofold degenerate e_g orbitals, corresponding to the operator ℓ_e. Because of the fast time scale of electron hopping, the hopping of an ℓ_e electron from a polaronic distorted site to a neighboring undistorted site is a nonadiabatic process leaving the local lattice distortion unrelaxed, and causes transitions to *high-energy intermediate states* of energy $\sim E_{JT}$. These are similar to the Frank-Condon processes in molecular physics. They can be taken into account by expressing the ℓ_e operator as a composite of the ℓ operator and the (inverse of the) Lang-Firsov transformation factor[44] that generates the phonon distortion that characterizes the polaron. (It is for the same reason that the *low-energy scale* quantum amplitudes for the hopping of the ℓ *polarons* to the neighboring sites are reduced by the exponentially small "Huang-Rhys" factor,[45] and become sizable only at energies of order E_{JT}.)

For the purposes of this paper, we model these processes in a way that captures their essential features while retaining simplicity in calculations by approximating them as single band Holstein polaronic states (i.e., ignoring the complexity of the Jahn-Teller and breathing mode phonon distortions that accompany the polarons in doped manganites). Then the Green's function for ℓ electrons is given by[42]

$$G_{\ell_e\ell_e}(\tau) = \exp[-\Phi(\tau)]G_{\ell_p\ell_p}(\tau),$$
$$\text{where } \Phi(\tau) = g_0[(N_{ph}+1)(1-e^{-\tau\omega_{ph}}) + N_{ph}(1-e^{\tau\omega_{ph}})],$$
$$N_{ph} = \frac{1}{e^{\beta\omega_{ph}}-1} \quad \text{with} \quad \beta \equiv \frac{1}{k_B T}, \quad (19)$$

$g_0 \equiv \frac{E_{JT}}{\omega_{ph}}$ is the dimensionless *electron-phonon coupling strength*, ω_{ph} is the frequency of the (Jahn-Teller/Holstein) phonons, and $G_{\ell_p\ell_p}(\tau)$ is the Green's function of the *polaron*. (Here and below we include the subscript p to denote polarons for clarity of presentation, although in the ℓ–b model we had not used this subscript, for notational simplicity.)

By using an explicit Matsubara representation of Eq. (19), followed by a Wick rotation to *real frequency*, we get the following expression for the spectral function of the ℓ electrons:

$$A_{l_el_e}(\omega) = e^{-g_0(2N_{ph}+1)}\left[A_{l_pl_p}(\omega) + \sum_{n=1}^{\infty} f_n\{A_{l_pl_p}(\omega - n\omega_{ph}) \times F_1(\omega,n\omega_{ph}) + A_{l_pl_p}(\omega + n\omega_{ph})F_2(\omega,n\omega_{ph})\}\right], \quad (20)$$

where

$$f_n = 2\sinh\left[\frac{\beta n\omega_{ph}}{2}\right] I_n\{2g_0\sqrt{N_{ph}(N_{ph}+1)}\}, \quad (21)$$

$$F_1(\omega,n\omega_{ph}) = 1 + \frac{1}{e^{\beta n\omega_{ph}}-1} - \frac{1}{e^{\beta(\omega-n\omega_{ph})}+1}, \quad (22)$$

$$F_2(\omega,n\omega_{ph}) = \frac{1}{e^{\beta n\omega_{ph}}-1} - \frac{1}{e^{\beta(\omega+n\omega_{ph})}+1}, \quad (23)$$

and $I_n(x)$ is the familiar modified Bessel function of order n. For the purposes of the present work, where $\ell-b$ hybridization effects are neglected, the polaronic Green's function is site diagonal. Furthermore, within the spirit of the dynamical mean-field treatment of $H_{\ell b}$, the polaronic spectral function $A_{l_p l_p}(\omega)$ is well approximated by the simple form[46]

$$A_{l_p l_p}(\omega) = \delta(\omega-\bar{\epsilon}_\ell), \quad \text{where} \quad \bar{\epsilon}_\ell = \epsilon^*_\ell - \mu, \quad (24)$$

where ϵ^*_ℓ is the fully self-consistent renormalized Jahn-Teller energy level that arises in the DMFT treatment.[16,17,37]

With this kind of polaronic spectral function we get the following exact analytical expressions for $\sigma_{\ell b}(\omega)$; $\sigma_{\ell b}(\omega) = \sigma^{(1)}_{\ell b}(\omega) + \sigma^{(2)}_{\ell b}(\omega)$, with $\sigma^{(1)}_{\ell b}(\omega)$ and $\sigma^{(2)}_{\ell b}(\omega)$ being given by

$$\sigma^{(1)}_{\ell b}(\omega) = C_{\ell b}\int_{-\infty}^{+\infty} d\epsilon\ D_0(\epsilon)\sum_\sigma\Bigg[A^\sigma_{bb}(\epsilon,\omega+\bar{\epsilon}_\ell)F_3(\omega,\bar{\epsilon}_\ell) + \sum_{n=1}^{\infty} f_n\big\{A^\sigma_{bb}(\epsilon,\omega+\epsilon^+_n)F_1(\epsilon^+_n,n\omega_{ph})F_3(\omega,\epsilon^+_n) + A^\sigma_{bb}(\epsilon,\omega+\epsilon^-_n)F_2(\epsilon^-_n,n\omega_{ph})F_3(\omega,\epsilon^-_n)\big\}\Bigg], \quad (25)$$

$$\sigma^{(2)}_{\ell b}(\omega) = C_{\ell b}\int_{-\infty}^{+\infty} d\epsilon\, D_0(\epsilon)\sum_\sigma\Bigg[A^\sigma_{bb}(\epsilon,\bar{\epsilon}_\ell-\omega)F_3(\omega,\bar{\epsilon}_\ell-\omega) + \sum_{n=1}^{\infty} f_n\big\{A^\sigma_{bb}(\epsilon,\epsilon^+_n-\omega)F_1(\epsilon^+_n,n\omega_{ph})F_3(\omega,\epsilon^+_n-\omega) + A^\sigma_{bb}(\epsilon,\epsilon^-_n-\omega)F_2(\epsilon^-_n,n\omega_{ph})F_3(\omega,\epsilon^-_n-\omega)\big\}\Bigg]. \quad (26)$$

Here, F_1 and F_2 are as defined earlier;

$$C_{\ell b} \equiv \sigma_0\pi^2\alpha^2_{\ell b}\bar{t}^2\exp[-g_0(2N_{ph}+1)],$$

$$F_3(\omega,\omega') = \frac{n_F(\omega')-n_F(\omega+\omega')}{\omega};$$

$$\epsilon^\pm_n \equiv \bar{\epsilon}_\ell \pm n\omega_{ph} \quad \text{and} \quad D_0(\epsilon) = \frac{2}{\pi D_0^2}\sqrt{D_0^2-\epsilon^2};$$

with $\sigma_0 \equiv e^2/(ha)$ ($\simeq 38.05\,(\mathrm{k\Omega\,cm})^{-1}$ for $a = 1$ Å) setting the basic scale of conductivity in the system, $\bar{t}$ being the hopping amplitude for the b electrons. The *zero frequency* or dc conductivities can be straightforwardly and separately calculated by taking the limit $\omega \to 0$ of $\sigma(\omega)$ and are explicitly given by the formulas

$$\sigma^{dc}_{bb} \equiv \sigma_{bb}(0) = -C_{bb}\int_{-\infty}^{+\infty} D_0(\epsilon)d\epsilon\int_{-\infty}^{+\infty} d\omega' \times\sum_\sigma\left[A^\sigma_{bb}(\epsilon,\omega')\right]^2 n'_F(\omega'), \quad (27)$$

$$\sigma^{dc}_{\ell b} \equiv \sigma_{\ell b}(0) = -C_{\ell b}\int_{-\infty}^{+\infty} D_0(\epsilon)d\epsilon\sum_\sigma\Bigg[A^\sigma_{bb}(\epsilon,\bar{\epsilon}_\ell)n'_F(\bar{\epsilon}_\ell) + \sum_{n=1}^{\infty} f_n\big\{A^\sigma_{bb}(\epsilon,\epsilon^+_n)F_1(\epsilon^+_n,n\omega_{ph})n'_F(\epsilon^+_n) + A^\sigma_{bb}(\epsilon,\epsilon^-_n)F_2(\epsilon^-_n,n\omega_{ph})n'_F(\epsilon^-_n)\big\}\Bigg], \quad (28)$$

where $n'_F(x) \equiv [\frac{dn_F(\omega)}{d\omega}]_{\omega=x}$, and $C_{bb} \equiv 2\sigma_0\pi^2\bar{t}^2$. For the purposes of the calculations we present in the next section, we treat D_0, J_F, and $\alpha_{\ell b}$ as adjustable parameters. We choose E_{JT} and U based on known estimates for the LaSr system. We adjust J_F and D_0 so as to recover the experimental magnetic transition temperature T_c and the resistivity at T_c.[37] We choose $\alpha_{\ell b} = 1$ but in general $\alpha_{\ell b} \leqslant 1$ (see the Appendix) for more details.

IV. RESULTS AND COMPARISON WITH EXPERIMENTS *VIS-À-VIS* OTHER THEORIES

The computation of the optical conductivity of the $\ell-b$ model using the above formalism is straightforward. First, for a given choice of the parameters of the model, picked as stated above, and of doping and temperature, the DMFT is carried out along the lines that have been well discussed elsewhere.[17,18,37] From such a calculation we obtain the b spectral function and the renormalized ℓ binding energy, ϵ^*_ℓ. From these we calculate the optical conductivities as above. We have carried out such calculations for a wide range of temperatures, and for several doping values.

As mentioned earlier and discussed in more detail later in this paper (see Sec. V), because of the neglect of the intersite $\ell-b$ coherence effects in the DMFT treatment presented here, σ_{bb} is greatly underestimated at low temperatures. Correcting this in a fully satisfactory way presents major theoretical challenges, and we address these issues elsewhere. For the purposes of this paper, we have tried to correct this in an *ad hoc* way by *boosting the contribution to the optical conductivity from the $b-b$ channel by a factor of 8*. This gives rise to dc conductivities close to the experimentally observed values reported in Ref. 7. As $\sigma_{\ell b}$ has its dominant contributions at relatively large frequencies, we expect that it will be affected very little by the neglect of the $\ell-b$ coherence effects, and hence we do not correct it. In the last section (Sec. V) of this paper we discuss issues related to $\ell-b$ coherence effects in greater detail.

First, we consider the canonical system $La_{1-x}Sr_xMnO_3$ ($x = 0.175$). This system is barely metallic ($x_c = 0.16$) and has a ferromagnetic ground state, which upon heating goes to a paramagnetic insulating state. We use the following parameters for our calculations: $D_0 = 1.245$ eV, $J_F = 72.5$ meV, $E_{JT} = 0.535$ eV, $\omega_{ph} = 75$ meV, and $U = 5$ eV. With these parameters the calculated magnetic transition temperature was found to be $T_c = 280$ K as compared to the experimental $T_c = 283$ K.

In Fig. 2 we have plotted $\sigma(\omega)$ at various temperatures as indicated. Broadly $\sigma(\omega)$ has features similar to those in the experimental data mentioned earlier, consisting of a coherent Drude-like peak in the far-infrared region ($\omega \to 0$) along with a broad peak in the mid-infrared region. In our

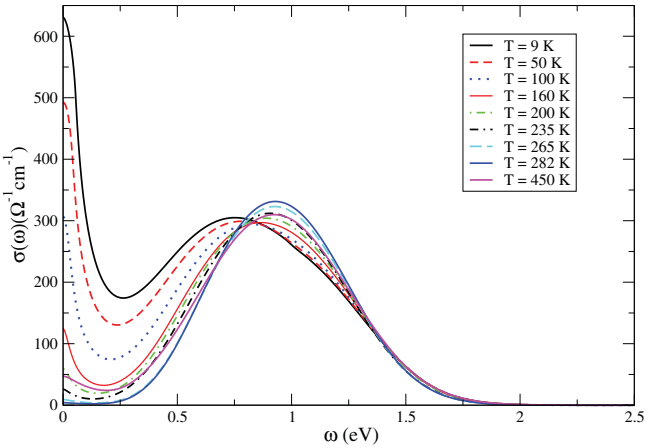

FIG. 2. (Color online) Optical conductivity, $\sigma(\omega)$, for the system $La_{1-x}Sr_xMnO_3$ at various temperatures as indicated, for $x = 0.175$.

calculations,the coherent Drude-like peak arises from the $b-b$ channel contribution $\sigma_{bb}(\omega)$, whereas the mid-infrared peak arises from the excitation of the polaronic states (ℓ electrons) present in the system. The position of the mid-infrared peak is at $\omega \sim 2E_{JT}$ and is comparable to the experimentally observed energy scale ($\sim$1.5 eV).

As we can see from Fig. 2 the height of the Drude peak decreases dramatically with increasing temperature up to T_c. But for temperatures above T_c there is slow building up of the Drude peak in the far-infrared region. Correspondingly, as can be observed from Fig. 3(b), the integrated spectral weight

$$I_{bb}(\omega_c) = \int_0^{\omega_c} \sigma_{bb}(\omega) d\omega$$

(with a cutoff frequency ω_c, set equal to 3.5 eV) also shows a similar kind of behavior and becomes extremely small near T_c. This is to be attributed to the fact that in the $\ell-b$ model, the effective b bandwidth shrinks with increasing temperature due to the increasing scattering from the t_{2g} core spins, which get increasingly disordered, its bottom eventually rising above the renormalized ℓ level leading to a metal-to-insulator transition at T_c; and consequently the average (thermodynamic) b-electron number per site, $\bar{n}_b$, decreases rapidly with increasing temperature up to T_c. $\bar{n}_b$ again increases slowly above T_c due to the increasing thermal excitation of carriers across the insulating gap, as can be observed from Fig. 3(a). Our results are very similar to what is seen in many doped manganites, and in particular to the experimental observations of Okimoto *et al.*[8] Furthermore, $\bar{n}_b$, as well as $I_{bb}(\omega_c)$, is not proportional to m^2, in contrast to what arises in a DMFT study of the pure double exchange (DE) model by Furukawa.[24]

On the other hand, the temperature evolution of mid-infrared peak is significantly different. As is clear from Fig. 2, with increasing temperatures up to T_c, the spectral weight under the coherent Drude peak gradually gets transferred to higher frequencies (mid-infrared region) whereas above T_c this trend gets reversed and there is a slow rebuilding of the coherent Drude peak. The integrated spectral weight

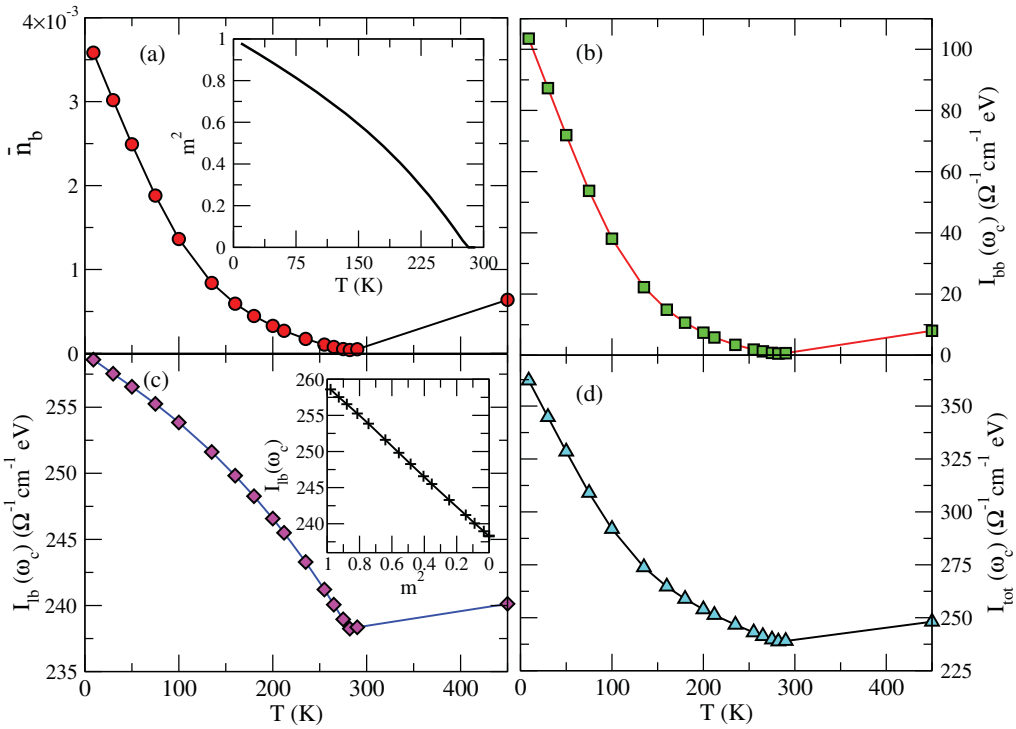

FIG. 3. (Color online) (a) Temperature variation of average (thermodynamic) b-electron number per site, $\bar{n}_b$. Inset: Temperature variation of square of magnetization, m^2. (b) Temperature variation of $I_{bb}(\omega_c)$ (see text for definition). (c) Same thing for $I_{\ell b}(\omega_c)$ Inset: Change in $I_{\ell b}(\omega_c)$ as a function of m^2. (d) Temperature variation of $I_{tot}(\omega_c) \equiv I_{bb}(\omega_c) + I_{lb}(\omega_c)$. All the calculations have been done for the system $La_{1-x}Sr_xMnO_3$ ($x = 0.175$).

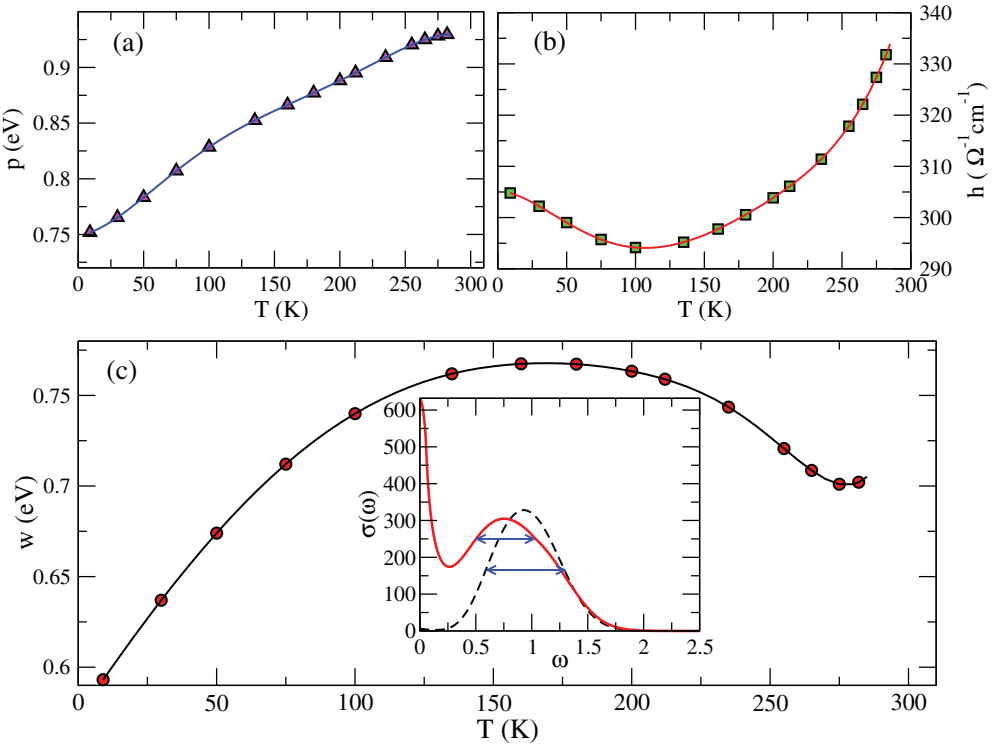

FIG. 4. (Color online) (a)–(c) Temperature variation of peak position (p), peak height (h), and peak width (w) of the mid-infrared peak for the system $La_{1-x}Sr_xMnO_3$ with $x = 0.175$. Inset ((c): Peak width of the mid-infrared peak has been indicated for two temperatures $T = 9$ K (solid line) and $T = 275$ K (dashed line).

from the $\ell - b$ channel,

$$I_{\ell b}(\omega_c) = \int_0^{\omega_c} \sigma_{\ell b}(\omega)\, d\omega,$$

decreases slightly with temperature up to T_c [Fig. 3(c)]. (Note the scale on the y axis; the total change is only about 7.5%.) More interestingly, the *slope* of the reduction in spectral weight is found to be proportional to m^2, the square of the local magnetization, as shown in the inset of Fig. 3(c). The height of the mid-infrared peak (h) as inferred from the *total conductivity* initially decreases with increasing temperature, due to rapid decrease of $\sigma_{bb}(\omega)$ and then increases slowly up to T_c, as shown in Fig. 4(b). The position of the peak (p) monotonically shifts toward higher frequencies with increasing temperature, mainly due to shift in local chemical potential μ [Fig. 4(a)]. The width of the peak (w), shown in [Fig. 4(c)], initially increases and reaches a saturation value $\sim$0.78 eV at around $T = 150$ K but eventually decreases near T_c.

We note that the *total integrated spectral weight* $I_{tot}(\omega_c)$, shown in Fig. 3(d), also decreases with increasing temperature, the temperature dependence of the decrease being clearly dominated by that of $I_{bb}(\omega_c)$. The apparent violation of the optical sum rules, particularly the f-sum rule,

$$\int_0^\infty \sigma(\omega)\, d\omega = -\pi e^2 \langle \tau^{xx} \rangle \equiv -\frac{\pi e^2}{2a} \int d\epsilon\, D_0(\epsilon)\epsilon \int \frac{d\omega}{\pi} n_F(\omega)\, \mathrm{Im}[G(\epsilon,\omega)], \tag{29}$$

is in itself interesting, and is characteristic of strongly correlated systems. It results from the transfer of spectral weights to very high energy scales, such as the upper Hubbard bands due to the changing occupancies of the polaronic levels, and the upper Hund bands due to the disorder in the t_{2g} spins, which we have not considered in the calculations above.

So far we have discussed the temperature variation of the optical conductivity spectra in the canonical system $La_{1-x}Sr_xMnO_3$ ($x = 0.175$). Next we discuss the doping dependence of optical conductivity spectra. We choose five $La_{1-x}Sr_xMnO_3$ systems with their doping values given by $x = 0.1, x = 0.14, x = 0.175, x = 0.24$, and $x = 0.3$. The first two samples have ferromagnetic insulating (FI) ground states and undergo transitions to paramagnetic insulating (PI) states upon heating. All the other samples have ferromagnetic metallic (FM) ground states, but upon heating undergo transitions either to paramagnetic insulating states (in the case of $x = 0.175$, $x = 0.24$) or to a paramagnetic metallic (PM) state (in the case of $x = 0.3$).

In our calculations, for all the systems we use the same set of parameters except for different ferromagnetic exchange coupling J_F (which, being generated by the virtual double exchange mechanism in our model, is indeed doping dependent). We choose $J_F = 40, 55, 72.5, 85.7$, and 92.5 meV for $x = 0.1$, $x = 0.14, x = 0.175, x = 0.24$, and $x = 0.3$, respectively. The calculated T_c's were found to be 150, 213, 280, 340, and 370 K, respectively, as compared to their experimental values 145, 215, 283, 338, and 369 K.

In Fig. 5 we have shown the doping dependence of total optical conductivity $\sigma(\omega)$ for a temperature $T = 9$ K.

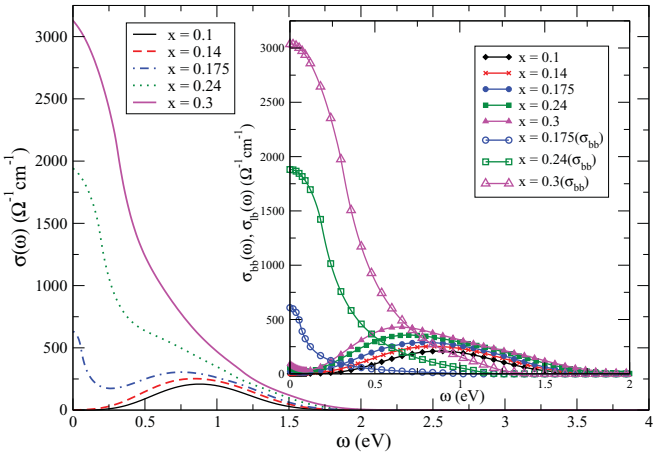

FIG. 5. (Color online) Doping dependence of $\sigma(\omega)$ at a fixed temperature $T = 9$ K for the system $La_{1-x}Sr_xMnO_3$. Inset: Contributions from $b-b$ and $\ell-b$ channels have been shown separately; open symbols for $\sigma_{bb}(\omega)$ and closed symbols for $\sigma_{\ell b}(\omega)$. $\sigma_{bb}(\omega)$ for insulating samples ($x = 0.1, x = 0.14$) are extremely small ($\leqslant 0.01$) and have not been shown in the figure.

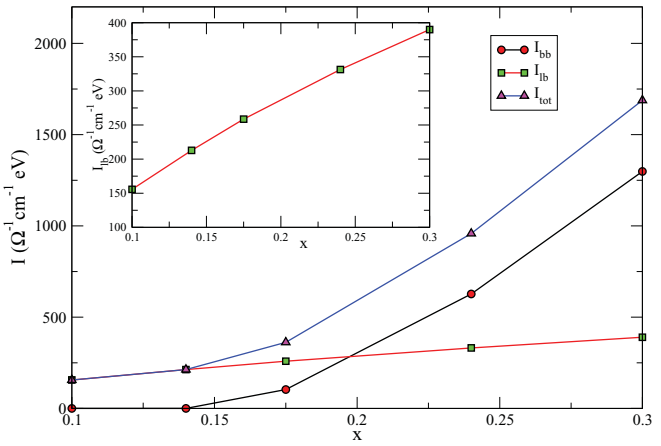

FIG. 6. (Color online) Integrated spectral weights at $T = 9$ K as a function of doping x for the system $La_{1-x}Sr_xMnO_3$. Inset : Detail variation of $I_{\ell b}$.

For systems with insulating ground states, the "coherent" Drude part in the far-infrared region is dramatically, but understandably, absent; and $\sigma(\omega)$ is completely dominated by the incoherent, broad, mid-infrared peak. This is due to the fact that in such systems the number of thermally excited b electrons is exponentially small (in our DMFT calculations[16] the the effective b band is so narrow due to the strong exclusion scattering from the ℓ polarons that its bottom is above the renormalized ℓ level, so that the b band is essentially empty except for the thermally excited carriers) and their contribution to $\sigma_{bb}(\omega)$ as well as $\sigma(\omega)$ is negligible. As we increase the doping the effective b bandwidth increases and the ground state of the system changes from a ferromagnetic insulating state to a ferromagnetic metallic state[16] at $x_c = 0.16$. As we have already discussed in the last section, for a barely metallic system ($x = 0.175$), $\sigma(\omega)$ consists of a far-infrared coherent Drude peak and an incoherent broad mid-infrared peak. As we increase the doping further the Drude peak height as well as spectral weight under the Drude peak increases substantially. For the optimally doped system ($x = 0.3$), the total conductivity $\sigma(\omega)$ is overwhelmingly dominated by the coherent Drude part. So, as we go from a deep insulating state ($x = 0.1$) to a good metallic state ($x = 0.3$) $\sigma(\omega)$ shows a crossover from the one dominated by the incoherent mid-infrared spectrum to that dominated by the coherent "Drude" spectrum.

The integrated spectral weights $I_{bb}(\omega_c)$, $I_{\ell b}(\omega_c)$, and $I_{\rm tot}(\omega_c)$ increase monotonically with increasing doping as can be observed from Fig. 6. However, the contribution from the $b-b$ channel $I_{bb}(\omega_c)$ increases dramatically above x_c as compared to $I_{\ell b}(\omega_c)$. We find that $I_{bb}(\omega_c)$ fits a doping dependence of the form $a(x - x_c) + b(x - x_c)^2$ for $x > x_c$; whereas the contribution from the $\ell-b$ channel $I_{\ell b}(\omega_c)$ as well as the total integrated spectral weight $I_{\rm tot}(\omega_c)$ in the insulating systems is proportional to the doping x (a similar result has been mentioned in the study by Chen *et al.*[33]). The peak height for $\sigma_{\ell b}(\omega)$ increases with x but the peak position shifts toward lower frequency as can be observed from inset of Fig. 5.

The above discussions show that our results are similar to those seen in a wide class of doped manganites, and in particular with the experimental observations from the Tokura group.[7,8] It is also fair that we compare and contrast our results with results from various earlier theoretical calculations of the optical conductivity of doped manganites. We do this in the rest of this section.

The pure double exchange model (which can be recovered from the $\ell-b$ model if E_{JT} is driven positive, so that there are no polarons in the system, all the electrons are mobile b electrons, and J_F is set to zero) was one of the earliest models that was proposed[47] as an explanation for the ferromagnetism seen in the manganites, and calculations of the optical conductivity have been made for this model within a DMFT framework.[24,30] For a finite J_H, in the ferromagnetic metallic (FM) state, $\sigma(\omega)$ indeed shows a *two*-peak structure consisting of a Drude-like peak arising from intraband transitions in the lower spin split (Hund) band, and a peak at $\omega \sim 2J_H$ arising from inter-Hund-band transitions, from the lower to the upper spin split band. However, by all accounts the relevant values of J_H appropriate to the manganites are around 2 eV, whence the position of this peak would not be consistent with the experimentally determined mid-infrared peak position at $\omega \sim 1-2$ eV. Also, the detailed temperature and doping dependence of $\sigma(\omega)$ for this model has not been reported, and is unlikely to be consistent with the data. But more seriously, for systems with ferromagnetic insulating (FI) ground states this model cannot be applied, as the pure double exchange model always has a FM ground state, and cannot describe FI ground states or FI to FM transitions as a function of doping.

Kumar and Majumdar[25] treated a similar, single orbital, double exchange model, but in the limit of infinitely strong Hund's coupling, and with *added quenched disordered site energies*, numerically on large clusters. Their calculated $\sigma(\omega)$, for temperatures $T \geqslant T_c$, shows only a Drude peak for the pure case, but acquires an incoherent mid-infrared peak in the presence of the quenched disorder, the scale of the peak position being determined by the strength of the disorder

potential. However, with increasing temperature the mid-infrared peak height in this work decreases, which is the opposite trend to that seen experimentally.

In a subsequent approach Kumar *et al.*[26] added Holstein phonons to the above-mentioned double exchange model. The phonons were treated as annealed *classical displacement* variables to which electrons are coupled through their local density n_i with a coupling strength λ. For sufficiently large λ they find that quenched disorder can promote the self-trapping of carriers in such a way that it can give rise to a (low-temperature) metal (M) to (high temperature) insulator (I) transition, whereas, in the absence of quenched disorder, i.e., in the pure Holstein–double exchange model one gets only M-M (for weak electron-phonon coupling) or I-I transitions (for strong electron-phonon coupling). Sen *et al.*[27] have considered essentially the same model with an added antiferromagnetic superexchange interaction between the core spins, as well as a more realistic (for manganites) two-orbital model. They have studied the properties of these models, again numerically, using exact diagonalization of the fermionic sector for a given configuration of the classical phonons and t_{2g} core spins, which configurations are then updated via a Monte Carlo simulation (MC) procedure, but on square lattices with fewer sites, up to 12×12, and find similar results. To the best of our knowledge no studies of optical conductivity in these models at a level comparable to what we have discussed in our paper have been reported so far for these models.

In all of these cases, the physics behind polaron formation is the localization of charge carriers arising due to the combination of the quenched disorder (whose source in the real materials is the random substitution of A-site cationic species), and the annealed disorder arising from the phonon displacements and the spin disorder. *Some* of the consequences arising from such *classical polaronic states*, and especially in the work by Kumar *et al.* and Sen *et al.*, are at a qualitative level not very different from those in the *two-fluid* $\ell-b$ model without the coherence effects, and thus are also consistent with several experimental features of the manganites.

However, although all doped manganites are indeed disordered, it is very unlikely that the disorder scales can be as large (eV) as required by these models in order for them to generate the experimentally observed features, for the quenched disorder potential arises from the dopant impurities, which are well away from the Mn sites, and there is evidence that it is strongly dielectrically screened even in the insulating manganites (see Ref. 22 for a discussion and references). Furthermore, they cannot explain certain important experimental results like the very strong isotope dependence of T_c, the sign reversal of Hall resistivity at low temperatures, etc., which depend crucially on the existence of the polaron-mobile electron coherence scale. The two-fluid model discussed here in principle includes the quantum dynamics of phonons in as much as it gives rise to the $\ell-b$ coherence effects (via the Huang-Rhys factor), although the detailed calculations presented in our paper have not included these coherence effects, and have focused more on the mid-infrared regime where the coherence effects are unlikely to play a prominent role.

Millis, Muller and Shraiman[28] were the first to emphasize the importance of including the Jahn-Teller electron-phonon coupling in models of manganites in order to obtain insulating states at finite doping. While their model included doubly degenerate e_g electrons coupled to both the Jahn-Teller modes (Q_2 and Q_3) the phonons were treated only as adiabatic or classical displacement variables, and without including co-operative JT effects. In a companion work,[29] t_{2g} core spins (treated classically as in our work) were included as well. The models were studied using DMFT, as here. They found that the model does indeed produce insulating states if the dimensionless electron-phonon coupling λ_{e-ph} is strong enough. However, there are no metal-to-insulator transitions with changes of doping or of temperature—if λ_{e-ph} is strong enough to generate an insulator at low doping, the system stays insulating for increased doping as well, and vice versa. Thermal transitions are also either metal to (bad) metal, or insulator to insulator (though in this case there are portions of the temperature-dependent resistivity at intermediate temperatures that "look metallic"). These limitations are also reflected in the optical conductivity (see Figs. 7 and 10 of Ref. 29)—$\sigma(\omega)$ has either a Drude peak or a mid-infrared peak, but one does not get both at low temperatures, with transfers of spectral weights as a function of doping or temperature, as seen experimentally and as obtained in our work.

Yunoki *et al.*[31] considered essentially the same model as in Ref. 29, but with an added antiferromagnetic exchange between the t_{2g} core spins. The model was studied *numerically*, using Metropolis Monte Carlo methods, on one-dimensional (1D) lattices of up to 22 sites, 2D cluster of size up to 4^2 sites, and 3D clusters of up to 4^3 sites, for temperatures down to $1/50$ (in units of t). The results found are qualitatively similar to those of Ref. 29. Optical conductivities were calculated only for the 1D models, it being suggested that the results in two and three dimensions would be similar. If λ_{e-ph} is not big enough (results shown for $\lambda_{e-ph} = 1$ and a doping of 0.3), $\sigma(\omega)$ has a Drude peak at low temperatures. As the temperature is increased, leading to a bad metal, the Drude peak drops, and a peak appears at finite frequency that gradually moves outwards to higher frequencies as T increases. Though these results share some features of the experimental observations of Takenaka *et al.*[12] they do not show the *two*-peak structure observed in the wide class of doped manganites. For large λ_{e-ph} (1.5), $\sigma(\omega)$ has what seems like a mid-infrared peak (at $\omega \sim 4t \sim 0.8$ eV for $x = 0$), but again, the peak moves to smaller frequencies with doping. This is again very different from the behavior seen in experiments and in our work.

The work of Allen and Perebeinos[32] comes the closest in spirit to the work we have presented in this paper. They used a model for the parent compound $LaMnO_3$, which is similar to that considered in Ref. 29, but keeping the coupling of the e_g electrons only to the Q_3 mode, corresponding to the orthorhombic Jahn-Teller distortions. However, they included cooperative JT effects, and intraorbital Coulomb correlation effects between the e_g electrons in the $U = \infty$ limit (which effectively projects out one orbital from the Hilbert space). The model was again studied with the electron-phonon coupling treated under an *adiabatic* approximation (i.e., treating the distortions as purely classical variables), the ground state of the system being inferred through an exact

diagonalization of the model on a lattice comprising of four unit cells. Some effects of quantized lattice vibrations were added heuristically (as we have done in the present work) subsequently, by arguing that if an additional hole is added on to this ground state then it can become site localized provided the electron-phonon interaction is strong enough and one treats various delocalization effects perturbatively. The calculated optical conductivity showed a mid-infrared peak arising due to Frank-Condon excitations of the phonon sidebands.

This work was later extended[33] to lightly hole doped systems ($x \sim 0.1$) and it was shown, by treating electron-phonon coupling in the Born-Oppenheimer approximation and various delocalization effects perturbatively, that the doped holes get self-trapped and hence give rise to nearly site localized small polaronic states. The optical spectra obtained from excitation of these again give rise to a mid-infrared peak, whose integrated spectral weight is proportional to doping. It is clear that this work contains several of the ingredients present in our model, and in a very similar spirit. However, the method of exact diagonalization is limited to small clusters and small doping regimes, and cannot access the doping driven magnetic and insulator-metal transitions, or the thermal transitions.

By contrast, in our work, by adding in a second fluid of mobile b electrons to such a fluid of polarons, including Coulomb interaction driven exclusion effects between the two fluids, and treating the model in the DMFT framework, we are able to understand all these as well as several other observed phenomena in manganites in a simple way, and perform calculations appropriate to bulk systems, with the results discussed above.

V. CONCLUSION AND PROSPECTS

In summary, in this paper we have presented a study of the temperature evolution as well as the doping dependence of the optical conductivity of doped rare-earth manganites based on the recently proposed two-fluid $\ell-b$ model. As shown in an earlier series of papers, with choices of parameters that are natural for these systems this model can reproduce the experimentally observed phase diagram for a significant doping range (e.g., $0.05 < x < 0.4$ for $La_{1-x}Ca_xMnO_3$ and $La_{1-x}Sr_xMnO_3$) and hence can be applied for systems with both metallic and insulating ground states.

In the first part of the presentation of our results we discussed the temperature dependence of $\sigma(\omega)$ for the canonical system $La_{1-x}Sr_xMnO_3$ ($x = 0.175$). This system has a ferromagnetic metallic ground state and goes to a paramagnetic insulating state upon heating. At low temperatures $\sigma(\omega)$ consists of a coherent Drude peak in the far-infrared region, arising from intraband transitions of b electrons, and a broad peak in the mid-infrared region, due to Frank-Condon-like excitations from polaronic states. This is a simple and natural explanation for the two-peak structure seen in several experimental findings. The energy scale of the peak position ($\omega \sim 2E_{JT}$) is also quite consistent with experiments. Upon heating the metallic system, the Drude peak as well as the spectral weight under this peak decreases quite rapidly as the b band gets depopulated due to the reduction of its effective bandwidth via double exchange induced scattering from the increasing disorder of the core spins. The high-temperature spectrum is therefore dominated by the mid-infrared peak only. The height of the mid-infrared peak initially decreases and then increases monotonically up to T_c and the position of the peak shifts to higher frequencies. The width of the peak initially increases, then nearly saturates at high temperatures, but eventually decreases near T_c. Most interestingly, with increasing temperature up to T_c spectral weight gets transferred from the far-infrared Drude region to the mid-infrared region, over energy scales that are much higher than k_BT. Above T_c the trend gets reversed.

In the second part we presented a systematic study of the doping dependence of $\sigma(\omega)$. We showed results for five different systems $x = 0.1$, $x = 0.14$, $x = 0.175$, $x = 0.24$, and $x = 0.3$. With a suitable choice of parameters we have reproduced magnetic transition temperatures T_c, close to experimental T_c. The first two systems have insulating ground states and the remaining systems have metallic ground states. For the insulating systems, corresponding to low x, $\sigma(\omega)$ consists only of the broad mid-infrared peak; the Drude peak is absent as only an exponentially small number of thermally activated mobile electrons populate the b band. As we increase the doping x the model shows a transition from insulating to metallic ground states at a critical doping x_c. On the metallic side b-electron numbers, and hence the integrated spectral weight, increase dramatically with increasing doping because of the increase in bandwidth ($D \propto \sqrt{x}$ for $U = \infty$) as well as the decrease in Coulomb correlation effects (reduced scattering from the decreasing number of ℓ electrons). Metallic systems close to x_c show a two-peak structure as has been discussed in the last paragraph but close to optimal doping $\sigma(\omega)$ is overwhelmingly dominated by the Drude part. So, with increasing doping $\sigma(\omega)$ shows a crossover from the mid-infrared dominated spectra to the Drude dominated spectra. All these trends are again in agreement with experiments in a wide class of manganites.

In the present paper we have refrained from making a detailed, quantitative comparison of the $\sigma(\omega)$ from our calculations with experimental data. The main reason is that, as pointed out elsewhere as well,[18,19,21] in the present study we have neglected the effect of intersite $\ell-b$ hybridization and the consequent coherence effects, which are especially important for the metallic systems for $\omega, k_BT \lesssim k_BT_{\rm coh}(\sim 5-10\,{\rm meV})$. This results in a much exaggerated scattering of the b electrons from the random distributions of the ℓ polarons down to the lowest temperatures, causing the overall size of our calculated dc conductivities (and hence also of the Drude conductivities) to be much smaller (i.e., the resistivities much larger) than what is observed in many manganites. Since σ_{bb} involves two b propagators, and $\sigma_{\ell b}$ only one, the exaggerated scattering of the b electrons does not affect the two quantities to the same degree. Furthermore, the dominant contributions to $\sigma_{\ell b}$ occur at mid-infrared frequencies, where the $\ell-b$ coherence effects are not operative. Hence to compensate partly for this, in this paper we boosted our calculated σ_{bb} by a factor of 8. However, to the extent that in the theory presented here we (1) do not yet have a microscopic theory for the possible doping and temperature dependence of this factor, or of the orbital correlations encoded in $\alpha_{\ell b}$ (see the Appendix), both

of which will affect the relative contributions of the Drude and the mid-infrared contributions to the total conductivity, (2) have taken the $J_H \to \infty$ limit, thereby suppressing the contributions to the optical conductivity from the upper Hund bands, the tails from which could contribute in the mid infrared region, and (3) have not included realistic band-structure effects, a detailed quantitative comparison might not be very meaningful. We note that the same $\ell-b$ coherence issues are also presumably responsible for the difference between the temperature and doping dependence of optical conductivities from samples with cleaved[12] versus polished[7,8] surfaces.[13] Our expectation is that the polishing of the surfaces generates substantial amount of stresses and oxygen disorder well into the bulk, suppressing $\ell-b$ coherence effects, and *rendering our calculations more applicable*. On the other hand, in very high quality single-crystal samples with cleaved surfaces and at doping values well into the metallic regime, the coherence effects could become sufficiently prominent so as to render the JT distortions dynamic, dramatically reduce polaronic effects, substantially increase the Drude peak, and suppress the mid-infrared contribution, as seen in the experiments by Takenaka.[12] Even within a DMFT framework, the inclusion of $\ell-b$ coherence effects is very challenging, as the effective impurity problem is no longer exactly soluble, and requires sophisticated techniques such as the numerical renormalization group (NRG).[41] We hope to address these effects in future work.

ACKNOWLEDGMENTS

N.P. would like to thank the JNCASR, Bangalore for financial support. T.V.R. and H.R.K. would like to acknowledge support from the DST, India, through the Ramanna and J. C. Bose Grants, respectively. H.R.K. would like to thank the KITP, UCSB, Santa Barbara for the hospitality and the environment that enabled him to complete a substantial part of the writing of this paper, and T.V.R. would like to acknowledge the hospitality of NCBS, Bangalore.

APPENDIX

For a system whose electronic states are labeled by orbital and spin indices, the expression for the current density operator j^μ on a lattice is given by

$$j^\mu = \frac{i}{2\hbar}\sum_{\langle i,j\rangle} t_{ij}^{\alpha\gamma} R_{ij}^\mu (a_{i\alpha\sigma}^\dagger a_{j\gamma\sigma} - a_{j\gamma\sigma}^\dagger a_{i\alpha\sigma}), \tag{A1}$$

where $R_{ij}^\mu = R_i^\mu - R_j^\mu$ is the μth component of the relative displacement vector $\mathbf{R}_{ij}$ between site i, described by $\mathbf{R}_i$, and a neighboring site j, described by $\mathbf{R}_j$, and the repeated Greek indices represent the orbital indices and are summed over. For manganites, the specifics of the relationship of the ℓ_e and b electron creation operators to the microscopic twofold degenerate e_g electron creation operators depend on the details of the modeling of the JT phonons, and are not of crucial importance for the purposes of this paper. For example, when the JT phonons are treated in an approximation which neglects the cooperative JT effects, then on the distorted sites,

$$b_{i\sigma}^\dagger \equiv \cos\left(\frac{\theta_i}{2}\right) a_{i1\sigma}^\dagger + \sin\left(\frac{\theta_i}{2}\right) a_{i2\sigma}^\dagger, \tag{A2}$$

$$\ell_{ei\sigma}^\dagger \equiv -\sin\left(\frac{\theta_i}{2}\right) a_{i1\sigma}^\dagger + \cos\left(\frac{\theta_i}{2}\right) a_{i2\sigma}^\dagger, \tag{A3}$$

where $\theta_i \equiv \tan^{-1}(Q_{2i}/Q_{3i})$ is an angle variable that determines the "orientation" of the local distortion in terms of the amplitudes of the two JT modes Q_{2i} and Q_{3i}. On the undistorted sites, among which the b electrons primarily move, $b_{i\sigma}^\dagger$ can then be any linear combination of the two e_g creation operators. We do not keep track of the orbital labels in this paper, assuming that they get averaged over in the "orbital liquid" doping regimes that we focus on in this paper. For a discussion of how one might treat these in contexts where orbital correlations are important, see Ref. 20.

It is important to mention that at a given distorted site if we express the electron phonon Hamiltonian, involving the twofold degenerate e_g electrons coupled to the two JT modes Q_{2i} and Q_{3i} whose dynamics is described by quantum mechanical phonons, then in the above basis $\{b_i,\ell_{ei}\}$, in the limit of strong electron-phonon coupling, $g_0(\equiv \frac{E_{JT}}{\omega_{ph}}) \gg 1$, we get the broad band (b_i) and polaronic (ℓ_i) states and subsequently in a lattice description the hopping amplitude of polaronic ℓ_i states get renormalized by the Huang-Rhys factor $\exp\{-E_{JT}/2\omega_{ph}\}$ (see Ref. 48 for more detail).

Now if we express the current operator j^μ in $b_{i\sigma}^\dagger$ and $\ell_{ei\sigma}^\dagger$ operators then we get

$$j^\mu = \frac{i}{2\hbar}\sum_{\langle i,j\rangle} R_{ij}^\mu\left[\alpha_{ij}^{bb}\left(b_{i\sigma}^\dagger b_{j\sigma} - b_{j\sigma}^\dagger b_{i\sigma}\right) + \alpha_{ij}^{\ell b}\left(\ell_{ei\sigma}^\dagger b_{j\sigma} - b_{j\sigma}^\dagger \ell_{ei\sigma}\right) + \alpha_{ij}^{b\ell}\left(\ell_{ei\sigma}^\dagger b_{j\sigma} - b_{j\sigma}^\dagger \ell_{ei\sigma}\right) + \alpha_{ij}^{\ell\ell}\left(\ell_{ei\sigma}^\dagger \ell_{ej\sigma} - \ell_{ej\sigma}^\dagger \ell_{ei\sigma}\right)\right]. \tag{A4}$$

Here onwards ℓ will correspond to ℓ_e unless mentioned otherwise. The various coefficients α_{ij}^{bb}, etc. are given by

$$\alpha_{ij}^{bb} = t_{ij}^{11}\cos\frac{\theta_i}{2}\cos\frac{\theta_j}{2} + t_{ij}^{22}\sin\frac{\theta_i}{2}\sin\frac{\theta_j}{2} + t_{ij}^{12}\cos\frac{\theta_i}{2}\sin\frac{\theta_j}{2} + t_{ij}^{21}\sin\frac{\theta_i}{2}\cos\frac{\theta_j}{2}, \tag{A5}$$

$$\alpha_{ij}^{\ell\ell} = t_{ij}^{11}\sin\frac{\theta_i}{2}\sin\frac{\theta_j}{2} + t_{ij}^{22}\cos\frac{\theta_i}{2}\cos\frac{\theta_j}{2} - t_{ij}^{12}\sin\frac{\theta_i}{2}\cos\frac{\theta_j}{2} - t_{ij}^{21}\cos\frac{\theta_i}{2}\sin\frac{\theta_j}{2}, \tag{A6}$$

$$\alpha_{ij}^{\ell b} = t_{ij}^{22}\cos\frac{\theta_i}{2}\sin\frac{\theta_j}{2} - t_{ij}^{11}\sin\frac{\theta_i}{2}\cos\frac{\theta_j}{2} + t_{ij}^{21}\cos\frac{\theta_i}{2}\cos\frac{\theta_j}{2} - t_{ij}^{12}\sin\frac{\theta_i}{2}\sin\frac{\theta_j}{2}, \tag{A7}$$

$$\alpha_{ij}^{b\ell} = t_{ij}^{22}\sin\frac{\theta_i}{2}\cos\frac{\theta_j}{2} - t_{ij}^{11}\cos\frac{\theta_i}{2}\sin\frac{\theta_j}{2} + t_{ij}^{12}\cos\frac{\theta_i}{2}\cos\frac{\theta_j}{2} - t_{ij}^{21}\sin\frac{\theta_i}{2}\sin\frac{\theta_j}{2}. \tag{A8}$$

We write down the contribution for $\chi^{\mu\nu}(i\omega_n)$ in various *incoherent* channels as

$$\chi^{\mu\nu}(i\omega_n) = \chi^{\mu\nu}_{bb}(i\omega_n) + \chi^{\mu\nu}_{\ell\ell}(i\omega_n) + \chi^{\mu\nu}_{\ell b}(i\omega_n) + \chi^{\mu\nu}_{b\ell}(i\omega_n). \tag{A9}$$

The "polarization bubble" in the $b-b$ channel is given by

$$\Pi^{\mu\nu}_{bb}(\tau) \propto \sum_{\langle i,j\rangle}\sum_{\langle m,n\rangle} R^{\mu}_{ij}R^{\nu}_{mn}\langle\alpha^{bb}_{ij}\alpha^{bb}_{mn}\rangle\big[G^{bb}_{mj\sigma}(\tau)G^{bb}_{in\sigma}(-\tau) - G^{bb}_{mi\sigma}(\tau)G^{bb}_{jn\sigma}(-\tau) - G^{bb}_{nj\sigma}(\tau)G^{bb}_{im\sigma}(-\tau) + G^{bb}_{ni\sigma}(\tau)G^{bb}_{jm\sigma}(-\tau)\big] \tag{A10}$$

and a similar term for the $\ell-\ell$ channel with b replaced by ℓ. For the off-diagonal channel $\ell-b$ we have

$$\begin{aligned}\Pi^{\mu\nu}_{\ell b}(\tau) \propto \sum_{\langle i,j\rangle}\sum_{\langle m,n\rangle} R^{\mu}_{ij}R^{\nu}_{mn}\big[&\langle\alpha^{\ell b}_{ij}\alpha^{b\ell}_{mn}\rangle\big\{G^{bb}_{mj\sigma}(\tau)G^{\ell\ell}_{in\sigma}(-\tau) + G^{\ell\ell}_{ni\sigma}(\tau)G^{bb}_{jm\sigma}(-\tau)\big\}\\ &-\langle\alpha^{\ell b}_{ij}\alpha^{\ell b}_{mn}\rangle\big\{G^{\ell\ell}_{mi\sigma}(\tau)\times G^{bb}_{jn\sigma}(-\tau) + G^{bb}_{nj\sigma}(\tau)G^{\ell\ell}_{im\sigma}(-\tau)\big\}\big].\end{aligned} \tag{A11}$$

Under *orbital liquid* (i.e., there is no long-range *orbital order*) approximation such terms will vanish unless indices m,n are not equal to indices i,j, etc.

Under single site DMFT approximation we express the various "polarization bubbles" in terms of site diagonal Green's functions involving two sites i and j as

$$\Pi^{\mu\nu}_{bb}(\tau) \propto -\sum_{\langle i,j\rangle} R^{\mu}_{ij}R^{\nu}_{ij}\langle\alpha^{bb}_{ij}\big(\alpha^{bb}_{ij}+\alpha^{bb}_{ji}\big)\rangle\big[G^{bb}_{ii\sigma}(\tau)G^{bb}_{jj\sigma}(-\tau) + G^{bb}_{jj\sigma}(\tau)G^{bb}_{ii\sigma}(-\tau)\big] \tag{A12}$$

and for the off diagonal $\ell-b$ channel

$$\Pi^{\mu\nu}_{\ell b}(\tau) \propto -\sum_{\langle i,j\rangle} R^{\mu}_{ij}R^{\nu}_{ij}\langle\alpha^{\ell b}_{ij}\big(\alpha^{\ell b}_{ij}+\alpha^{b\ell}_{ji}\big)\rangle\big[G^{\ell\ell}_{ii\sigma}(\tau)G^{bb}_{jj\sigma}(-\tau) + G^{bb}_{jj\sigma}(\tau)G^{\ell\ell}_{ii\sigma}(-\tau)\big] \tag{A13}$$

and similar expression for $\Pi^{\mu\nu}_{b\ell}(\tau)$ with the replacement $b \leftrightarrow \ell$. $\langle\cdots\rangle$ represents average over thermal and orbital degrees of freedoms. We now write down orbital dependant various hopping matrix elements for manganites,

$$t^{11}_{x} = -\sqrt{3}t^{12}_{x} = -\sqrt{3}t^{21}_{x} = 3t^{22}_{x} = \frac{3t_0}{4}, \tag{A14}$$

$$t^{11}_{y} = \sqrt{3}t^{12}_{y} = \sqrt{3}t^{21}_{y} = 3t^{22}_{y} = \frac{3t_0}{4}, \tag{A15}$$

$$t^{11}_{z} = t^{12}_{z} = t^{21}_{z} = 0; \quad t^{22}_{z} = t_0. \tag{A16}$$

By explicitly putting the matrix elements we get

$$\Pi^{xx/yy}_{bb}(\tau) \propto -\sum_{\langle i,j\rangle}\big(R^{x/y}_{ij}\big)^2\left[\frac{5t_0^2}{4}\xi_{ij} + \frac{3t_0^2}{4}\zeta_{ij}\right]\big[G^{bb}_{ii\sigma}(\tau)G^{bb}_{jj\sigma}(-\tau) + G^{bb}_{jj\sigma}(\tau)G^{bb}_{ii\sigma}(-\tau)\big], \tag{A17}$$

$$\Pi^{zz}_{bb}(\tau) \propto -\sum_{\langle i,j\rangle}\big(R^{z}_{ij}\big)^2 2t_0^2\xi_{ij}\big[G^{bb}_{ii\sigma}(\tau)G^{bb}_{jj\sigma}(-\tau) + G^{bb}_{jj\sigma}(\tau)G^{bb}_{ii\sigma}(-\tau)\big], \tag{A18}$$

and for the off-diagonal process we will get

$$\Pi^{xx/yy}_{\ell b}(\tau) \propto -\sum_{\langle i,j\rangle}\big(R^{x/y}_{ij}\big)^2\left[\frac{5t_0^2}{4}\zeta_{ij} + \frac{3t_0^2}{4}\xi_{ij}\right]\big[G^{\ell\ell}_{ii\sigma}(\tau)G^{bb}_{jj\sigma}(-\tau) + G^{bb}_{jj\sigma}(\tau)G^{\ell\ell}_{ii\sigma}(-\tau)\big], \tag{A19}$$

$$\Pi^{zz}_{\ell b}(\tau) \propto -\sum_{\langle i,j\rangle}\big(R^{x/y}_{ij}\big)^2 2t_0^2\zeta_{ij}\big[G^{\ell\ell}_{ii\sigma}(\tau)G^{bb}_{jj\sigma}(-\tau) + G^{bb}_{jj\sigma}(\tau)G^{\ell\ell}_{ii\sigma}(-\tau)\big], \tag{A20}$$

where

$$\left\langle\cos^2\frac{\theta_i}{2}\cos^2\frac{\theta_j}{2}\right\rangle = \xi_{ij} = \left\langle\sin^2\frac{\theta_i}{2}\sin^2\frac{\theta_j}{2}\right\rangle, \tag{A21}$$

$$\left\langle\cos^2\frac{\theta_i}{2}\sin^2\frac{\theta_j}{2}\right\rangle = \zeta_{ij} = \left\langle\sin^2\frac{\theta_i}{2}\cos^2\frac{\theta_j}{2}\right\rangle. \tag{A22}$$

Evaluation of ξ_{ij} and ζ_{ij} requires detail modeling of the short-range orbital correlation effects and is beyond the scope of the simplistic $\ell-b$ model used here.

However if we assume that the orbital correlations are only nearest neighbor and translationaly invariant then we can replace ξ_{ij} and ζ_{ij} by its nearest-neighbor constant values ξ_0 and ζ_0. For such a case we can parametrize ξ_0 and ζ_0 by a single parameter α as

$$\xi_{ij} = \xi_0 = \tfrac{1}{4}(1+\alpha) \quad \text{and} \quad \zeta_{ij} = \zeta_0 = \tfrac{1}{4}(1-\alpha). \tag{A23}$$

The ratio between the *diagonal* (b−b) and *off-diagonal* (ℓ−b,b−ℓ) channels (averaged over all three directions) is then $\lambda = \frac{2-\alpha}{2+\alpha}$. Hence the *diagonal* and *off-diagonal* channels contribute to the total optical conductivity in the ratio $1:\lambda$. The prefactor $\alpha_{\ell b}$, appearing in Eq. (9) for current density operator $j^{\mu}_{\ell b}$, is simply then $\sqrt{\lambda}$.

---

*Present address: Department of Physics, Georgetown University, Washington, DC 20057.

[1] S. Jin *et al*., Science **264**, 413 (1994).

[2] *Colossal Magnetoresistance, Charge Ordering and Related Properties of Manganese Oxides*, edited by C. N. R. Rao and B. Raveau (World Scientific, Singapore, 1998).

[3] *Colossal Magnetoresistance Oxides*, edited by Y. Tokura (Gordon and Breach, New York, 2000).

[4] M. B. Salamon and M. Jaime, Rev. Mod. Phys. **73**, 583 (2001).

[5] E. Dagotto, T. Hotta, and A. Moreo, Phys. Rep. **344**, 1 (2001).

[6] G. H. Jonker and J. H. van Santen, Physica **16**, 337 (1950); G. H. Jonker, *ibid*. **22**, 707 (1956).

[7] Y. Okimoto, T. Katsufuji, T. Ishikawa, A. Urushibara, T. Arima, and Y. Tokura, Phys. Rev. Lett. **75**, 109 (1995).

[8] Y. Okimoto, T. Katsufuji, T. Ishikawa, T. Arima, and Y. Tokura, Phys. Rev. B **55**, 4206 (1997).

[9] K. H. Kim, J. H. Jung, and T. W. Noh, Phys. Rev. Lett. **81**, 1517 (1998).

[10] J. H. Jung, K. H. Kim, H. J. Lee, J. S. Ahn, N. J. Hur, T. W. Noh, M. S. Kim, and J.-G. Park, Phys. Rev. B **59**, 3793 (1999).

[11] H. J. Lee, J. H. Jung, Y. S. Lee, J. S. Ahn, T. W. Noh, K. H. Kim, and S.-W. Cheong, Phys. Rev. B **60**, 5251 (1999).

[12] K. Takenaka, Y. Sawaki, and S. Sugai, Phys. Rev. B **60**, 13011 (1999).

[13] The optical conductivity is determined by electromagnetic waves, which penetrate to a distance of the order of the skin depth δ, which is typically $\approx$100 Å; thus the property measured is a bulk one since the lattice constant $a \approx 2$−5 Å so that $\delta \gg a$. However, it is well known that the properties of manganites are sensitive to surface conditions; e.g., thin films show T_c quite different from those of the bulk up to thicknesses of order 200 Å. The polishing process probably creates stresses and oxygen defects that penetrate many layers into the bulk. This could be the underlying cause for the difference between the two sets of measurements. This issue has been addressed experimentally by Lee *et al*. (Ref. 11). We also note that Fig. 2 in Ref. 7 shows a "flat response" beyond the Drude region at low temperatures rendering the mid-infrared peak somewhat weak in comparison. However, this flat region seems to disappear when the temperature-independent contribution, attributed by the authors of Ref. 7 to interband transitions, is subtracted out (compare Figs. 2 and 3 of Ref. 7), also and does not seem to be a prominent feature in several other, later, optical conductivity results reported by the Tokura group [e.g., see Fig. 25 in Y. Tokura, Rep. Prog. Phys. **69**, 797 (2006)]. For some additional comments, see the concluding section.

[14] Ch. Hartinger, F. Mayr, A. Loidl, and T. Kopp, Phys. Rev. B **73**, 024408 (2006).

[15] P. Gao, T. A. Tyson, Z. Liu, M. A. DeLeon, and C. Dubourdieu, Phys. Rev. B **78**, 220404(R) (2008).

[16] G. Venketeswera Pai, S. R. Hassan, H. R. Krishnamurthy, and T. V. Ramakrishnan, Europhys. Lett. **64**, 696 (2003).

[17] T. V. Ramakrishnan, H. R. Krishnamurthy, S. R. Hassan, and G. Venkateswara Pai, Phys. Rev. Lett. **92**, 157203 (2004).

[18] T. V. Ramakrishnan, H. R. Krishnamurthy, S. R. Hassan, and G. Venketeswera Pai, in *Colossal Magnetoresistive Manganites*, edited by T. Chatterji (Kluwer Academic, Dordrecht, 2004).

[19] H. R. Krishnamurthy, Pramana-J. Phys. **64**, 1063 (2005).

[20] O. Cepas, H. R. Krishnamurthy, and T. V. Ramakrishnan, Phys. Rev. Lett. **94**, 247207 (2005); Phys. Rev. B **73**, 035218 (2006).

[21] T. V. Ramakrishnan, J. Phys.: Condens. Matter **19**, 125211 (2007).

[22] V. B. Shenoy, T. Gupta, H. R. Krishnamurthy, and T. V. Ramakrishnan, Phys. Rev. Lett. **98**, 097201 (2007); Phys. Rev. B **80**, 125121 (2009).

[23] P. Sanyal, S. SenGupta, N. Pakhira, H. R. Krishnamurthy, D. D. Sarma, and T. V. Ramakrishnan, Europhys. Lett. **82**, 47010 (2008).

[24] N. Furukawa, J. Phys. Soc. Jpn. **64**, 3164 (1995).

[25] S. Kumar and P. Majumdar, Phys. Rev. Lett. **91**, 246602 (2003); Eur. Phys. J. B **46**, 315 (2005).

[26] S. Kumar and P. Majumdar, Phys. Rev. Lett. **96**, 016602 (2006).

[27] C. Sen, G. Alvarez, and E. Dagotto, Phys. Rev. Lett. **98**, 127202 (2007).

[28] A. J. Millis, R. Mueller, and B. I. Shraiman, Phys. Rev. B **54**, 5389 (1996).

[29] A. J. Millis, R. Mueller, and B. I. Shraiman, Phys. Rev. B **54**, 5405 (1996).

[30] A. Chattopadhyay, A. J. Millis, and S. Das Sarma, Phys. Rev. B **61**, 10738 (2000).

[31] S. Yunoki, A. Moreo, and E. Dagotto, Phys. Rev. Lett. **81**, 5612 (1998).

[32] P. B. Allen and V. Perebeinos, Phys. Rev. Lett. **83**, 4828 (1999); Phys. Rev. B **60**, 10747 (1999).

[33] Y.-R. Chen, V. Perebeinos, and P. B. Allen, Phys. Rev. B **65**, 205207 (2002).

[34] Within the *single site* dynamical mean-field theory (DMFT) approximation used in the above-mentioned work both these temperatures are the same.

[35] A. E. Bocquet, T. Mizokawa, T. Saitoh, H. Namatame, and A. Fujimori, Phys. Rev. B **46**, 3771 (1992).

[36] S. Satpathy, Z. S. Popović, and F. R. Vukajlović, Phys. Rev. Lett. **76**, 960 (1996).

[37]S. R. Hassan, Ph.D. thesis, Indian Institute of Science, Bangalore, 2003.

[38]The superexchange coupling between the Mn core spins is of the order t^2/U or t^2/Δ_{pd}, where t, U are as defined earlier and Δ_{pd} is the charge-transfer energy between Mn and O sites, and can be antiferromagnetic or ferromagnetic depending on the orbital indices [A. J. Millis, Phys. Rev. B **55**, 6405 (1997)]. The virtual double exchange (VDE) mediated ferromagnetic coupling is of the order of $(t^2/E_{JT})x(1-x)$. For manganites U and Δ_{pd} are of the order 5 eV while E_{JT} is of the order $0.25-0.5$ eV, so for large doping VDE mediated ferromagnetic exchange is much larger than the superexchange term. In the present study we concentrate mainly on the ferromagnetic metallic state with doping range up to optimal doping and hence we can safely neglect the superexchange term. However, in the low doping regime, which we do not focus on in our paper, the competition between the two mechanisms gives rise to various magnetic phases, and a proper treatment of the optical conductivity in these regimes would indeed require the inclusion of the superexchange terms.

[39]L. M. Falicov and J. C. Kimball, Phys. Rev. Lett. **22**, 997 (1969).

[40]A. Georges, G. Kotliar, W. Krauth, and M. J. Rozenberg, Rev. Mod. Phys. **68**, 13 (1996).

[41]For more details, see N. Pakhira, Ph.D. thesis, Indian Institute of Science, Bangalore, 2008.

[42]G. D. Mahan, *Many Particle Physics* (Kluwer Academic/Plenum, New York, 2000).

[43]Th. Pruschke, D. L. Cox, and M. Jarrell, Europhys. Lett. **21**, 593 (1993); Phys. Rev. B **47**, 3553 (1993).

[44]I. G. Lang and Y. A. Firsov, Zh. Eksp. Teor. fiz. **43**, 1843 (1962) [Sov. Phys. JETP **16**, 1301 (1962)].

[45]K. Huang and F. Rhys, Proc. R. Soc. London, Ser. A **204**, 406 (1950).

[46]Even within the DMFT for the model ignoring the $\ell-b$ hybridization, the ℓ spectrum is actually not simple, and has x-ray singularities (e.g., see the analogous discussions in Ref. 23). We ignore such complications here, as any singularities in the spectra will be smeared out by the disorder present in these systems, and may not be easy to observe experimentally.

[47]C. Zener, Phys. Rev. **82**, 403 (1951); P. W. Anderson and H. Hasegawa, *ibid*. **100**, 675 (1955).

[48]G. V. Pai, Ph.D. thesis, Indian Institute of Science, Bangalore, 2001.